Journal of Alloys and Compounds 489 (2010) 488–492

Contents lists available at ScienceDirect

Journal of Alloys and Compounds

journal homepage: www.elsevier.com/locate/jallcom

Effect of current density on deposition process and properties of nanocrystalline Ni–Co–W alloy coatings

M.A. Farzaneh, K. Raeissi*, M.A. Golozar

Department of Materials Engineering, Isfahan University of Technology, Isfahan 84156-83111, Iran

ARTICLE INFO

Article history:
Received 20 July 2009
Received in revised form 5 September 2009
Accepted 7 September 2009
Available online 25 September 2009

Keywords:
Ni–Co–W alloy
Coating
Electrodeposition
EIS
Nanocrystalline
Corrosion resistance

ABSTRACT

The nanostructure Ni–Co–W alloy coatings were electrodeposited onto a copper substrate using different applied current densities, in a modified Watts-type bath. The coatings were single-phase solid solutions with average grain sizes about 6–11 nm, calculated from X-ray diffraction patterns using the Scherrer equation. EIS results showed that the adsorption and reduction of W-containing ion complexes dominated at all applied current densities. However, the diffusion of the ion complexes reached to a limitation at higher current densities. The W and Co contents of the coatings decreased with an increase in the applied current density. A homogeneous nodular surface morphology was obtained at all current densities. The coatings produced at low current densities, containing higher amount of alloying elements, showed lower corrosion resistance.

1. Introduction

The electrodeposited Ni–Co coating is an important engineering material widely used in various applications of magnetic devices, especially in micro-system technologies to manufacture sensors, actuators, micro-relays and inductors [1]. The electrodeposited Ni–W coating exhibits higher hardness and scratch resistance as compared with the finest pure nanocrystalline Ni alloys, although the contribution of solid-solution strengthening from W is expected to be essentially negligible [2]. In fact, interest in the electroplating of W-containing alloys stems from the tendency to enhance the hardness and also the corrosion resistance of the coating [3]. Regarding the characteristics of Co–W alloy that possesses interesting catalytic properties, but shows lower corrosion resistance, nickel is added into the bath to improve the corrosion resistance of coatings produced [4]. On the other hand, it has been reported that introducing W into Ni–Co coatings improves durability, hardness and resistance to high temperatures [3].

For the first time, the ternary Ni–Co–W coating was utilized in the production of magnetic-film memories, just because of its desirable soft magnetic properties. This coating also found wide applications in surface micromachining as well as magnetic or magneto resistive [5], heat conductive [6], good wear resistance and electrocatalytic activity [7]. No any reference could be traced out in the literature for electrodeposition of this ternary alloy except the results presented by Singh et al. [8].

The aim of this work is to study the electrodeposition mechanism of Ni–Co–W alloys by electrochemical impedance spectroscopy (EIS) technique. Factors influencing amounts of W and Co content, morphology and corrosion resistance of the coatings are also studied.

2. Materials and experimental procedures

Copper substrate was used in disk shape with 0.85 cm^2 surface area. The substrate was mechanically polished up to 1200 grade abrasive paper and then electropolished in a solution containing 65 wt% phosphoric acid and 35 wt% distilled water for 15 min. Ni–Co–W alloy was electrodeposited from a modified Watts-type bath at 25 °C. The composition of the bath is shown in Table 1. The number of coulombs passed for all coatings was kept constant at 36 C. According to Faraday's law, this should lead to a coating thickness of about 13 μm. The coating thickness was also measured on cross sections of the coated samples which confirmed the prediction of Faraday's law.

Electrodeposition cell used consisted of three electrodes; a copper cathode electrode, a platinum wire as an anode and a saturated calomel electrode (SCE) as a reference. Using dilute NaOH or dilute sulfuric acid, the pH of the bath was adjusted at 7.5.

In order to investigate the mechanism of electrodeposition, EIS measurements were carried out at dc potentials which were selected based on the cathodic scan reading. These potentials were −1170, −1220, −1250, −1300, −1540 and −1640 mV. In order to measure the impedances, an ac responser (EG&G model 1025) was coupled with a potentiostat (EG&G model 263A). For corrosion testing, variation of potential (E) vs. current density ($\log i$) was recorded after 30 min immersion of the coatings in 3.5 wt% NaCl solution at room temperature, using the above-mentioned potentiostat and a standard corrosion cell with graphite counter electrode and SCE as a reference electrode. The scan rate used was 1 mV s^{-1}.

* Corresponding author. Fax: +98 311 391 2752.
E-mail address: k_raeissi@cc.iut.ac.ir (K. Raeissi).

0925-8388/$ – see front matter © 2009 Elsevier B.V. All rights reserved.
doi:10.1016/j.jallcom.2009.09.092

Table 1
Composition of the bath and electrodeposition parameters used for Ni–Co–W electrodeposition.

$NiSO_4 \cdot 6H_2O$	Ni source	Magnitude
$CoSO_4 \cdot 7H_2O$	Co source	3.4
NaBr	Improves conductivity	15.5
NH_4Cl	Improves faradic efficiency	26.7
$C_8H_5Na_3O_7 \cdot 2H_2O$	Complexing reagent	178.6
$Na_2WO_4 \cdot 2H_2O$	W source	50
pH		7.5
Current densities		2.5, 5, 7.5, 15, 50 and 70 mA cm^{-2}

A WEGA TESCAN scanning electron microscope (SEM) was used to study the coatings morphology. The presence of W and Co in the coatings was determined by EDS coupled with SEM. The grain size of the coatings was determined from X-ray diffraction patterns obtained by a diffractometer (Philips model X'pert). The grain size was calculated using the angular width of the nickel (1 1 1) peak at its Full-width at Half Maximum (FWHM) in conjunction with the Scherrer formula [9] given by Eq. (1):

$$\frac{0.9\lambda}{\beta \cos \alpha} \quad (1)$$

where λ, β and α are the wavelength of Cu Kα ($\lambda = 1.5406$ Å), the integral width and the diffraction angel, respectively. The four-parameter Gaussian function was used for curve fitting analysis required for FWHM determination. Instrumental line broadening was measured by a silicon standard specimen and corrected by the Gaussian–Cauchy equation. Wang et al. have been shown that the grain size measured by the Gaussian–Cauchy equation is similar to what is obtained by TEM observation [10].

3. Results and discussion

3.1. Deposition current densities

Suitable current densities for electrodeposition were selected based on the cathodic scan plot (Fig. 1). As it can be seen, by decreasing the cathodic potential, within the range of −500 to −800 mV (region I), the current density remains almost constant. This potential range is most probably related to the limitation arises due to predominant hydrogen evolution. In this way, hydroxide species may be formed by hydrolysis due to the local pH increase near the cathode surface [11]. For coating deposition, the current densities of 2.5, 5, 7.5 and 15 mA cm^{-2} were selected from the linear portion on cathodic scan (region II) and 50 and 70 mA cm^{-2} from region III. These current densities correspond to the potentials of −1170, −1220, −1250, −1300, −1540 and −1640 mV, respectively.

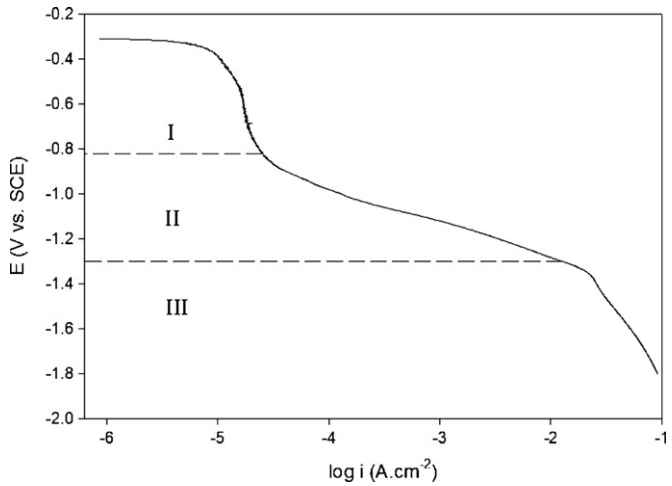

Fig. 1. Cathodic polarization plot (scan rate = 40 mV s^{-1}).

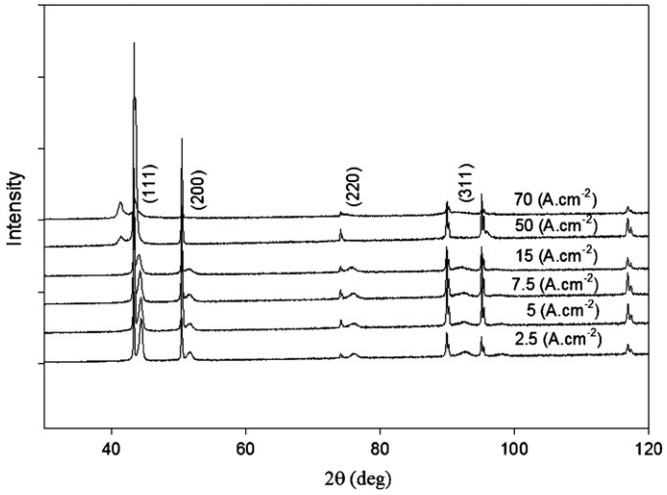

Fig. 2. XRD patterns of Ni–Co–W coatings produced at various current densities.

3.2. Grain size determination

X-ray diffraction patterns of the as-deposited Ni–Co–W alloy coatings are shown in Fig. 2. From the obtained patterns, a solid solution of face-centered cubic (fcc) structure is deduced for Ni–Co–W coating. Table 2 shows the grain size, as well as the Co and W contents of the coatings obtained at mentioned current densities. The results indicate that the coatings consist of nanocrystalline grains. In spite of increasing the deposition current density, grain size remains almost constant (6–11 nm), but the Co and W contents of the deposits decreases significantly.

3.3. Electrochemical aspects of deposition

In order to investigate the electrochemical aspects of nanocrystalline formation during the electrodeposition process, EIS tests were performed at −1170, −1220, −1250, −1300, −1540 and −1640 mV in deposition bath. Nyquist plots obtained at these potentials are shown in Fig. 3. As it is seen in this figure, three time constants can be distinguished at the applied cathodic potentials. The first time constant, which appears as a small capacitive loop at very high frequencies, belongs to the formation and adsorption of a surface oxide film. This loop is also observed in Ni–W electrodeposition according to the results obtained by Kabi et al. [12]. The second time constant, which appears as a large capacitive loop at medium frequencies, results from double layer capacitance parallel to charge transfer resistance. The third time constant, which appears at low frequencies, is a second capacitive loop. This capacitive loop which appears at lower potentials should be due to the slow bulk diffusion of electrochemical active species which participate in electrodeposition process.

Regarding the mechanism of tungsten deposition proposed by Imanaga et al. [13], the high-frequency capacitive loop observed on the Nyquist plots can be an evidence for intermediate tungsten oxide formation [12]. On the other hand, the capacitive loop

Table 2
The grain size, Co and W percentage of coatings.

i (mA cm^{-2})	E (mV)	Grain size (nm)	Co (wt%)	W (wt%)
2.5	−1170	10	10.9	27.7
5	−1220	6	10.2	26.3
7.5	−1250	6	7.6	20.4
15	−1300	8	6.2	17.2
50	−1540	10	4.0	11.6
70	−1640	11	2.3	6.8

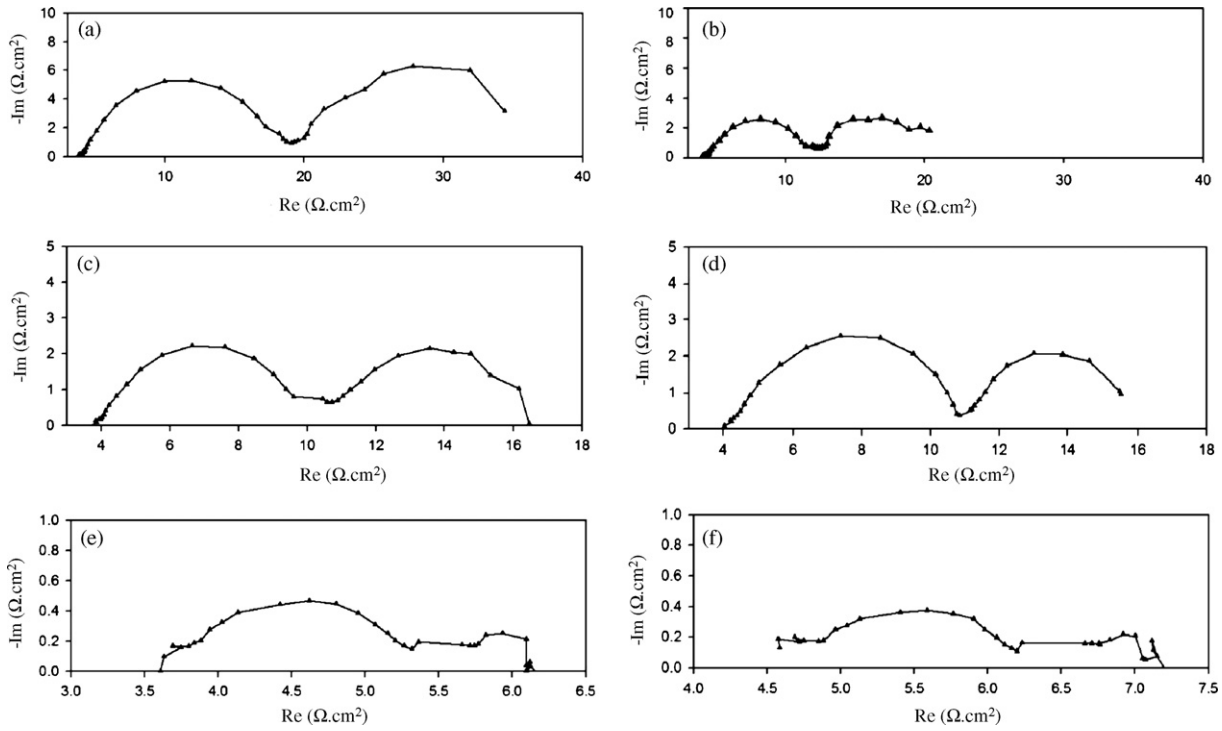

Fig. 3. Nyquist plots for Ni–Co–W electrodeposition at (a) −1170 mV, (b) −1220 mV, (c) −1250 mV, (d) −1300 mV, (e) −1540 mV and (f) −1640 mV.

which appears at low frequencies should be due to the slow bulk diffusion of electrochemical active species, which participate in electrodeposition process [12]. The low-frequency capacitive loop is in coincidence with the mechanism of tungsten deposition proposed by Younes et al. [14]. The electrochemical active species are the complex ions introduced as: $[(WO_4)(H)_n(Cit)]^{5-n}$, $[(Ni)(WO_4)(H)(Cit)]^{2-}$ [2,13,15] and also $[(WO_4)(H)(Cit)(H)_3]^{2-}$ [16]. According to the mechanism proposed by Younes and Gileadi [15], deposition of tungsten occurs through the reduction reactions which proceed through the production of some complexes in the bulk of solution. As the concentration of the complexes in the bath solution is very low, it can cause mass transport limitation for deposition process [16]. This phenomena is observed as a low-frequency capacitive loop as seen in Fig. 3.

According to the results obtained in this work, it can be concluded that both mechanisms proposed for tungsten deposition are valid. It seems that the mechanism of tungsten deposition is strongly under influence of diffusion rate of W-contained complex ions at higher current densities. In region III, the low-frequency capacitive loop is somewhat scattered, which confirms that the limitations arise during the diffusion of complex ions in the bulk solution.

Table 3 summarizes the corresponding values of charge transfer resistance (R_{ct}) and double layer capacitance (C_{dl}) extracted from Nyquist plots in Fig. 3. The values of R_{ct} were extracted from the Nyquist plots by direct fitting a circle onto the medium-frequency capacitive loop. The diameter of this circle is considered as R_{ct}. As it is seen from Fig. 4, R_{ct} is decreased by increasing the current density. The decrease of R_{ct} may be related to an increase in the surface diffusion of adions [17]. It has been proposed that a typical charge transfer takes place via three steps: (1) ion transfer from double layer to terrace sites and its adsorption, (2) surface diffusion of adsorbed ions (adions) on terrace sites, and (3) surface diffusion of adions on step-edge sites to the suitable active sites for reduction [18]. It is well known that increasing the surface diffusion of adions, which can be obtained by increasing the deposition current density [19], would facilitate their flux to the active growing sites and thus accelerate the grain growth. Therefore, higher rates of grain growth and consequently larger grains are expected at lower cathodic potentials (i.e. at higher current densities).

Table 3
The C_{dl} and R_{ct} data extracted from Nyquist plots in Fig. 3.

i (mA cm^{-2})	C_{dl} (μF cm^{-2})	R_{ct} (Ω cm^2)
2.5	282	14.21
5	462	7.20
7.5	549	5.80
15	728	3.68
50	999	1.51
70	1008	1.32

Reduction in grain size maybe due to a higher overpotential, which accompanies an increase in the nucleation rate [18]. Crystallization of Ni in an electrodeposition process usually involves two steps [20–22]. The first step is the discharge of nickel ions and generation of nickel atoms. There are two scenarios in the second step: (1) the incorporation of nickel atoms into the crystals and thus crystal growth and (2) the formation of new nucleus when the rate of crystal growth may not be sufficient to cater for generation of atom [23]. It has been shown that the critical radius of the surface nucleus is a function of the overpotential [23], the higher the overpotential is, the smaller the nucleus radius and thus the higher the nucleation rate would be. Therefore, with an increase in the current density, a higher overpotential, an accompanying increase in nucleation frequency and a reduction in the grain size could be achieved.

As it was discussed, parameters which increase the nucleation rate would decrease the grain growth and vice versa. It seems that a special condition is governed during the deposition of Ni–Co–W coating which allows a constant grain size to be obtained at all current densities (Table 2).

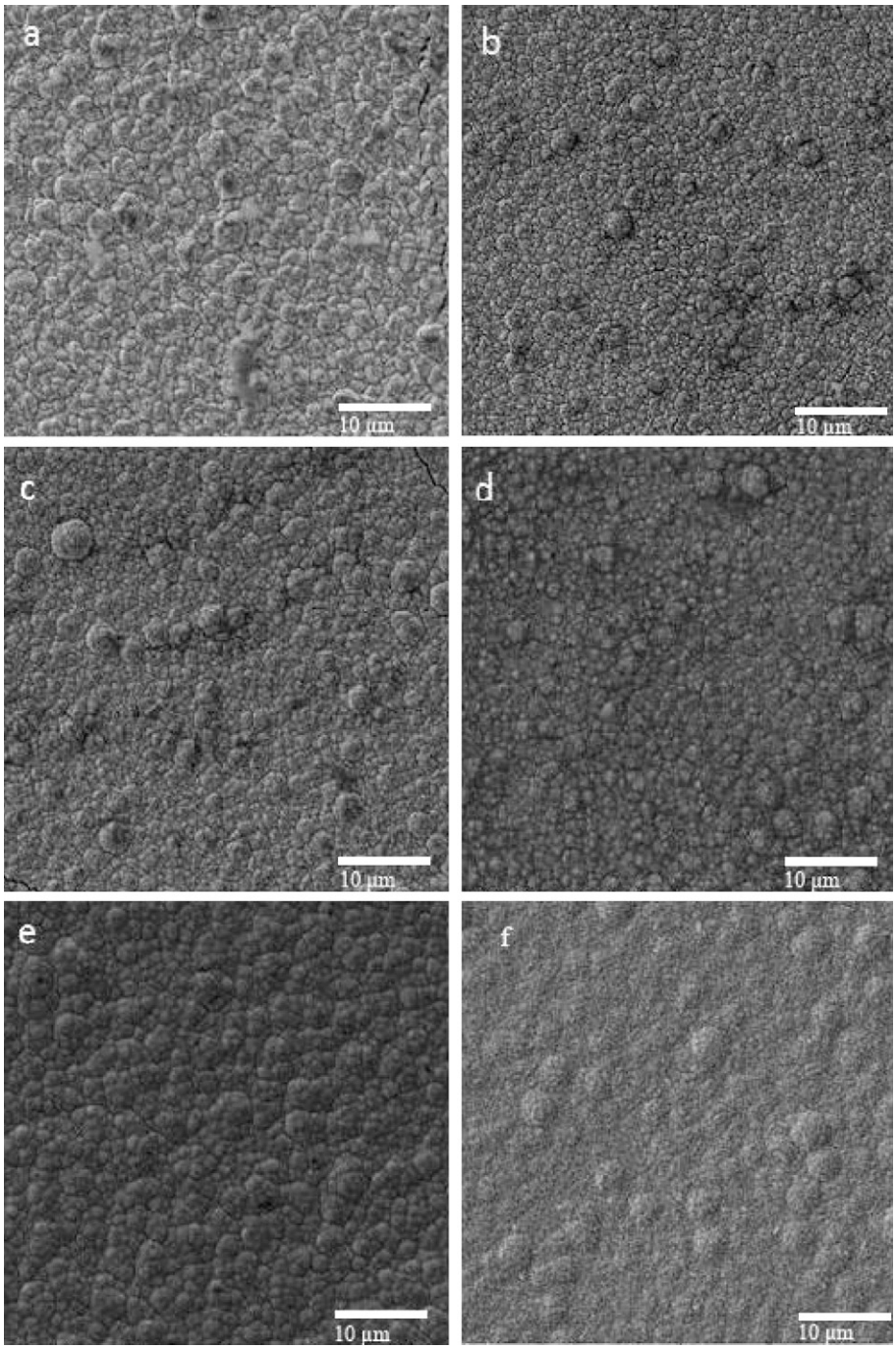

Fig. 4. SEM micrographs of Ni–Co–W coatings produced at (a) 2.5 mA cm^{-2}, (b) 5 mA cm^{-2}, (c) 7.5 mA cm^{-2}, (d) 15 mA cm^{-2}, (e) 50 mA cm^{-2} and (f) 70 mA cm^{-2}.

3.4. Morphology of coatings

Fig. 4 shows the SEM micrographs of the coatings produced at different current densities.

At all current densities, a colony-like morphology which consists of a lot of grain colonies having various sizes is seen. Each colony could be found to contain several smaller grains. The Ni–Co–W coatings are produced with some smaller ellipsoid-shaped globules appearing on top of the larger globules. The borders of these smaller and bigger globules are circular or quasi-circular, which is quite unlike the polygonal form of polycrystals, indicating the absence of grain boundaries [14]. Similar results have also been published previously [14,23].

3.5. Corrosion resistance of coatings

Fig. 5 shows the Tafel plots (E vs. $\log i$) of the coatings obtained at different current densities. Table 4 shows the related parameters extracted from the plots using Tafel extrapolation method. It is seen that a higher corrosion resistance (lower corrosion current density) is obtained for the coatings produced in the region III (around 2 μA cm^{-2}). As seen (Table 4), coatings produced at current densities in the region II, show higher corrosion current density. The highest corrosion current density is 4 μA cm^{-2} which is obtained for the coating deposited at 2.5 mA cm^{-2}. For the coating deposited at 5 mA cm^{-2}, the lowest corrosion potential (−500 mV vs. SCE) was obtained, which is most probably due to the finer surface morphology (Fig. 4b).

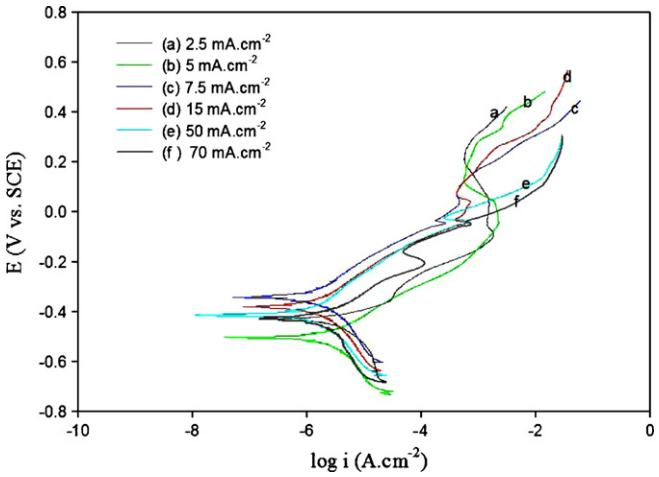

Fig. 5. Tafel polarization plots of Ni–Co–W coatings.

Table 4
Extracted parameters from E vs. log i plots in Fig. 5.

i (mA cm^{-2})	i_{corr} (μA cm^{-2})	E_{corr} (mV)	β_c (mV decade^{-1})	β_a (mV decade^{-1})
2.5	4 ± 2	−430	215.6	72.8
5	3.5 ± 0.8	−500	318.4	136.9
7.5	3 ± 0.5	−340	338.2	167.8
15	2.5 ± 1	−379	376.7	165.6
50	2 ± 1	−413	310.2	165.8
70	2 ± 1.5	−427	398.6	167.5

It is seen that the least corrosion rate is obtained for the coatings contain low amount of alloying elements (Co and W). According to the research work published by Obradovic et al. [24], alloys of Ni–W coatings having lower tungsten content show lower corrosion resistance. It has been mentioned that coatings with lower W content provide a fine-grain surface structure with no cracks which lead to more corrosion resistance [25]. Conversely, higher corrosion resistance has been reported for Ni–Co coatings with higher cobalt content [26]. This indicates the contrary effects of Co and W elements on the corrosion resistance of Ni–Co–W alloys.

4. Conclusions

1. Increasing the deposition current density would decrease the W and Co contents of Ni–Co–W coatings.
2. In spite of increasing the deposition current density, grain size of the Ni–Co–W coatings remained constant at 6–11 nm.
3. The highest corrosion resistance was obtained for the coatings produced at high current densities (region III on cathodic polarization reading). It seems that the contrary effects of Co and W elements determine the corrosion resistance of Ni–Co–W coatings.

References

[1] D. Golodnitsky, Yu. Rosenberg, A. Ulus, Electrochim. Acta 47 (2002) 2707–2714.
[2] C.A. Schuh, T.G. Nieh, H. Iwasaki, Acta Mater. 51 (2003) 431–443.
[3] O. Younes-Metzler, L. Zhu, E. Gileadi, Electrochim. Acta 48 (2003) 2551–2562.
[4] C. Santana, A. Regina, N. Campos, J. Mater. Sci. 42 (2007) 9137–9144.
[5] E. Gómez, S. Pané, X. Alcobe, E. Vallés, Electrochim. Acta 51 (2006) 5703–5709.
[6] B. Chi, J.B. Li, X.Z. Yang, Y.L. Gong, N. Wang, Int. J. Hydrogen Energy 30 (2005) 29–34.
[7] L. Wang, Y. Gao, Q. Xue, H. Liu, T. Xu, Appl. Surf. Sci. 242 (2005) 326–332.
[8] V.B. Singh, L.C. Singh, P.K. Tikoo, J. Electrochem. Soc. 127 (1980) 590.
[9] B.D. Cullity, S.R. Stock, Elements of X-ray Diffraction, Addison-Wesley, London, 2001.
[10] L. Wang, et al., Scripta Mater. 55 (2006) 657–660.
[11] A. Sanaty-Zadeh, K. Raeissi, A. Saidi, J. Alloys Compd. 485 (2009) 402–407.
[12] S. Kabi, K. Raeissi, A. Saatchi, J. Appl. Electrochem. 39 (2009) 1279–1285.
[13] H. Imanaga, J. Chem. Soc. Jpn. 63 (1960) 1336.
[14] O. Younes, L. Zhu, Y. Rosenberg, Y. Shacham-Diamand, E. Gileadi, Langmuir 17 (2001) 8270–8275.
[15] O. Younes, E. Gileadi, Electrochem. Solid-State Lett. 3 (2000) 543–545.
[16] M.D. Obradovic, R.M. Stevanovic, A.R. Despic, J. Electroanal. Chem. 552 (2003) 185–196.
[17] L. Wang, Y. Gao, T. Xu, Q. Xue, Mater. Chem. Phys. 99 (2006) 96–103.
[18] S. Hassani, K. Raeissi, M.A. Golozar, J. Appl. Electrochem. 38 (2008) 689–694.
[19] M. Holm, T.J. O'Keefe, J. Appl. Electrochem. 30 (2000) 1125–1132.
[20] A.M. El-Sherik, U. Erb, J. Page, Surf. Coat. Technol. 88 (1997) 70–78.
[21] G. Qiao, et al., Electrochim. Acta 51 (2005) 85–92.
[22] N.S. Qu, D. Zhu, K.C. Chan, W.N. Lei, Surf. Coat. Technol. 168 (2003) 123–128.
[23] Y. Li, H. Jiang, W. Huang, H. Tian, Appl. Surf. Sci. 254 (2008) 6865–6869.
[24] M. Obradovic, J. Stevanovic, A. Despic, R. Stevanovic, J. Stoch, J. Serb. Chem. Soc. 66 (2001) 899–912.
[25] Z. Galikova, M. Chovancova, V. Danielik, Chem. Pap. 60 (2006) 353–359.
[26] Sh. Hassani, Nickel–cobalt nanocrystalline coatings: electrodeposition mechanism and corrosion/tribo-corrosion behavior, M.Sc. Thesis, Isfahan University of Technology, Isfahan, 2008.